

Precise determination of the properties of $X(3872)$ and of its isovector partner W_{c1}

Teng Ji^{1,*}, Xiang-Kun Dong^{1,†}, Feng-Kun Guo^{2,3,4,5,‡}, Christoph Hanhart^{6,§} and Ulf-G. Meißner^{1,6,4,¶}

¹*Helmholtz Institut für Strahlen- und Kernphysik and Bethe Center for Theoretical Physics, Universität Bonn, D-53115 Bonn, Germany*

²*CAS Key Laboratory of Theoretical Physics, Institute of Theoretical Physics, Chinese Academy of Sciences, Beijing 100190, China*

³*School of Physical Sciences, University of Chinese Academy of Sciences, Beijing 100049, China*

⁴*Peng Huanwu Collaborative Center for Research and Education, Beihang University, Beijing 100191, China*

⁵*Southern Center for Nuclear-Science Theory (SCNT), Institute of Modern Physics, Chinese Academy of Sciences, Huizhou 516000, China*

⁶*Institute for Advanced Simulation (IAS-4), Forschungszentrum Jülich, D-52425 Jülich, Germany*

We perform a simultaneous fit to BESIII data on $e^+e^- \rightarrow \gamma(D^0\bar{D}^{*0}\pi^0/J/\psi\pi^+\pi^-)$ and LHCb data on $B^+ \rightarrow K^+(J/\psi\pi^+\pi^-)$ to precisely determine the properties of the $X(3872)$, with full consideration of three-body effects from $D^* \rightarrow D\pi$ decay, respecting both analyticity and unitarity. The $X(3872)$ is determined to be a bound state with a significance of 6σ , and its pole is located at $E_X = (-53_{-24}^{+9} - i34_{-12}^{+2})$ keV, relative to the nominal $D^0\bar{D}^{*0}$ threshold. Moreover, we confirm the presence of an isovector partner state, W_{c1} . It is found as a virtual state at $(1.6_{-0.9}^{+0.7} + i1.4_{-0.6}^{+0.3})$ MeV relative to the D^+D^{*-} threshold on an unphysical Riemann sheet, strongly supporting a molecular nature of both $X(3872)$ and W_{c1} . As a highly non-trivial prediction we show that the W_{c1} leads to nontrivial lineshapes in $B^0 \rightarrow K^0X(3872) \rightarrow K^0D^0\bar{D}^0\pi^0$ and $K^0J/\psi\pi^+\pi^-$ —thus the scheme presented here can be tested further by improved measurements.

INTRODUCTION

Since over 20 years the study of exotic hadronic states is one of the central themes in hadron physics. These states, which lie beyond the conventional quark model for quark-antiquark mesons and three-quark baryons, offer a unique opportunity to understand the inner workings of quantum chromodynamics (QCD), since different multi-quark configurations mean different realizations of confinement: In molecular states, confinement happens in the smallest possible subsystems, typically conventional hadrons, which are then bound together via a residual strong force, analogously to the binding of nucleons in nuclei; however, in the compact tetraquark picture, confinement is the binding force among all possible quark-(anti)quark pairs. The new quest was initiated by the discovery of $X(3872)$ in B decays [1], also denoted as $\chi_{c1}(3872)$ [2] after the quantum numbers were fixed to $J^{PC} = 1^{++}$ [3, 4]. The state was shortly after confirmed in various other experiments, and a growing family of exotic hadron candidates has since been reported experimentally and investigated theoretically; see Refs. [5–14] for recent reviews. The $X(3872)$ continues to serve as a benchmark for testing theoretical frameworks and constraining models of hadronic structure.

Despite the large number of experimental and theoretical studies, several aspects of $X(3872)$ remain poorly understood. Although the $X(3872)$ mass has been measured with high precision— $3871.64(6)$ MeV according to the 2024 issue of the Review of Particle Physics [2]—it remains unclear whether it lies above or below the $D^0\bar{D}^{*0}$ threshold, as the uncertainty encompasses this boundary. Notably, the mass and width of $X(3872)$ listed in

Ref. [2] are from averaging values extracted using the Breit-Wigner parameterization (e.g., in Refs. [15–17]), which is not appropriate for describing $X(3872)$ lineshape near the $D^0\bar{D}^{*0}$ threshold, a channel to which $X(3872)$ couples strongly in S -wave. While the Flatté parameterization of Ref. [18] employed in Refs. [19, 20] offers improvement by including the nonanalyticity at the $D^0\bar{D}^{*0}$ threshold, it neglects the three-body effects of the $D\bar{D}\pi$ system, as discussed in Refs. [21–25] for similar systems, which could hinder a precise determination of the $X(3872)$ properties. It also has the drawback that it assumes the coupled-channel potential matrix to be non-invertible and thus might not be sufficiently general [26–31]. Furthermore, another potentially crucial factor is missing in all existing analyses: In Ref. [25], it was shown using chiral effective field theory that data call for the existence of an isovector partner of $X(3872)$, there and here called W_{c1} —according to the naming scheme in Ref. [2] it should be $T_{c\bar{c}1}(3882)$ due to its quantum numbers $I^G(J^{PC}) = 1^-(1^{++})$.¹ The charged members of the same multiplet appear as virtual states in $(D\bar{D}^*)^\pm$ scattering. Their existence is supported by a recent lattice QCD calculation [32]. The neutral W_{c1}^0 manifests itself as a mild cusp at the D^+D^{*-} threshold whose strength is expected to be much weaker than the peak around the $D^0\bar{D}^{*0}$ threshold [25], which, however, distorts the lineshape and contaminates the signal of $X(3872)$.

Therefore, in order to extract the $X(3872)$ (and W_{c1}) properties reliably, it is necessary to reanalyze the data in

¹ Not to be confused with the $T_{c\bar{c}1}(3900)$, also known as $Z_c(3900)$, with quantum numbers $1^+(1^{+-})$.

a coupled-channel framework allowing for both states and including three-body effects. The results of this program are presented in this Letter.

FRAMEWORK

The $X(3872)$ couples mainly to the open-charm $D^0\bar{D}^{*0}$ and D^+D^{*-} channels² (labeled by the Greek index $\alpha=0, \pm$) as indicated by the large branching ratio into $D^0\bar{D}^{*0}$ reported in Refs. [20, 33–36] despite the tiny phase space—the statement remains true even with the revised branchings extracted in this work. It can also decay into several weakly coupled inelastic hidden-charm channels, such as $J/\psi\rho^0$, $J/\psi\omega$, $\chi_{cJ}\pi^0$ ($J = 0, 1, 2$), $J/\psi\gamma$, $\psi'\gamma$ and probably others. To analyze the existing data in the very limited energy region near the $D^0\bar{D}^{*0}$ and D^+D^{*-} thresholds, leading-order chiral effective field theory can be employed. At this order, the $D^0\bar{D}^{*0}$ - D^+D^{*-} coupled-channel scatterings are in S -waves, and the S - D wave mixing effects do not enter. Because there are no common valence quark flavors in charmonia and light mesons, rescatterings within the inelastic channels can be neglected due to Okubo-Zweig-Iizuka suppression.

The $D^0\bar{D}^{*0}$ - D^+D^{*-} coupled-channel scattering amplitude is derived from the Lippmann-Schwinger equation (LSE),

$$T_{\alpha\beta}(E; p', p) = V_{\alpha\beta}(E; p', p) + \int_0^\Lambda \frac{l^2 dl}{2\pi^2} V_{\alpha\mu}(E; p', l) G_{\mu\nu}(E; l) T_{\nu\beta}(E; l, p), \quad (1)$$

where E is the center-of-mass (c.m.) energy relative to the $D^0\bar{D}^{*0}$ threshold, p (p') is the magnitude of the incoming (outgoing) momentum, and Λ is a hard cutoff. G is the diagonal matrix of two-body propagators,

$$G_{\alpha\beta}(E; l) = \frac{\delta_{\alpha\beta}}{E - \Delta_{\alpha 0} - \frac{l^2}{2\mu_\alpha} + \frac{i}{2}[\Gamma_\alpha(E; l) + \Gamma_\alpha^{\text{rad}}]}, \quad (2)$$

with $\Delta_{\alpha 0}$ the threshold difference between channel- α and channel-0 and μ_α the reduced mass of particles in channel- α . The D^* decay widths take the $D\pi$ self-energies into account via the energy-dependent $\Gamma_\alpha(E; l)$, which introduces the $\pi D\bar{D}$ three-body cut into the amplitude, and the constant $\Gamma_\alpha^{\text{rad}}$ is accounting for the radiative $D\gamma$ partial width of D^* (see Refs. [22, 25] for explicit expressions).

The potential is constructed as

$$V(E; p', p) = V^{\text{ct}} + V^\pi(E; p', p) + V^{\text{inel}}(E). \quad (3)$$

V^{ct} is the constant contact interaction, which in channel space reads [37]

$$V^{\text{ct}} = \frac{1}{2} \begin{pmatrix} C_{0X} + C_{1X} & C_{0X} - C_{1X} \\ C_{0X} - C_{1X} & C_{0X} + C_{1X} \end{pmatrix}, \quad (4)$$

with C_{0X} and C_{1X} the isoscalar and isovector low-energy constants, respectively. The one-pion-exchange potential, V_π , introduces an additional three-body cut into the calculation necessary for theoretical consistency of the formalism [21, 22, 25]. V^{inel} accounts for effects of the inelastic channels that $X(3872)$ and its isovector partner W_{c1}^0 can couple to. This can be done in a way consistent with unitarity [38, 39], which gives

$$V_{\alpha\beta}^{\text{inel}}(E) = -i \sum_{j=\rho, \omega} \int_{-\infty}^{\infty} v_{\alpha j}(s) \rho_j(E, s) v_{\beta j}^*(s) \varrho_j(s) ds, \quad (5)$$

where the Latin indices $j = \rho, \omega$ represent the channels $J/\psi\rho$, $J/\psi\omega$, respectively. Note that V^{inel} is purely imaginary, since the corresponding real part has been absorbed into V^{ct} . The phase space factor is $\rho_j(E, s) = 4m_{J/\psi} m_j q_{j\text{cm}}(E, s) / (8\pi E)$, with $q_{j\text{cm}}$ the magnitude of c.m. momentum in channel- j and \sqrt{s} the invariant mass of the light quark system. The vector-meson spectral function,

$$\varrho_j(s) = -N_j \text{Im}[G_j(s)], \quad (6)$$

accounts for the finite width effects of the ρ, ω mesons, where N_j is fixed via the normalization $\int ds \varrho_j(s) = 1$. We take the ω propagator of the Breit-Wigner type, $G_\omega(s) = (s - m_\omega^2 + im_\omega\Gamma_\omega)^{-1}$ with $\Gamma_\omega = 8.68$ MeV [2], while for G_ρ , we use the best available spectral function in terms of the Omnès function [40], as done in Ref. [41]. The transitions of elastic channels to inelastic channels are parameterized as

$$v_{\alpha j}(s) = (1 + as) u_{\alpha k} \begin{pmatrix} 1 & \epsilon_{\rho\omega} G_\rho(s) \\ \epsilon_{\rho\omega} G_\omega(s) & 1 \end{pmatrix}_{kj}, \quad (7)$$

where $u_{\alpha k}$ are bare couplings. The renormalized ones, due to isospin symmetry, satisfy

$$u_{0\rho}^R = u_{0\omega}^R = -u_{\pm\rho}^R = u_{\pm\omega}^R, \quad (8)$$

where $u_{\alpha k}^R = \mathcal{G}_{\alpha\alpha} u_{\alpha k}$ with $u_{\pm\rho}$ a free parameter to be fitted and $\mathcal{G}_{\alpha\alpha} = \int_0^\Lambda \frac{l^2 dl^2}{2\pi^2} G_{\alpha\alpha}(0; l)$. We have introduced a first order polynomial in s as in Refs. [42, 43], and the slope a is a parameter to be determined from the fit. The ρ - ω mixing is covered by the off-diagonal element with $\epsilon_{\rho\omega} = 3.35(8) \times 10^{-3} \text{ GeV}^2$ [41]. For inelastic channels other than $J/\psi\rho^0$ and $J/\psi\omega$, the phase space factors are approximately constants in the narrow energy region

² Here and in the following, we use $D^0\bar{D}^{*0}$ and D^+D^{*-} to refer to the combinations with $J^{PC} = 1^{++}$. The $\bar{D}D^*$ components are included in the calculation but not written explicitly for simplicity.

of interest, and they also contribute to the imaginary part of the potential. However, since the experimental data [16, 20] have sizable energy resolutions, $\mathcal{O}(1 \text{ MeV})$, much larger than the imaginary part of the $X(3872)$ pole as determined by LHCb [19] and BESIII [20], such constant inelastic contributions can hardly be fixed by fitting to the currently available data. Therefore, we exclude these contributions in the baseline fit and assess their impact by introducing a constrained imaginary to evaluate variations in parameter values.

With the amplitudes solved from Eq. (1), the production of channel- α from a given $J^{PC} = 1^{++}$ source can be constructed as

$$U_\alpha(E, p) = P_\alpha + \int_0^\Lambda \frac{l^2 dl}{2\pi^2} P_\mu G_{\mu\nu}(E, l) T_{\nu\alpha}(E; l, p), \quad (9)$$

where P_α is the direct production amplitude of the neutral or charged $D\bar{D}^*$ channel. Then the production amplitudes of $D^0\bar{D}^0\pi^0$ and $J/\psi\pi^+\pi^-$ read

$$\begin{aligned} \mathcal{A}_{D^0\bar{D}^0\pi^0}(E, p, \bar{p}) &= U_\alpha(E, p)F_\alpha(p) + U_\alpha(E, \bar{p})F_\alpha(\bar{p}), \\ \mathcal{A}_{J/\psi\pi^+\pi^-}(E, s) &= \int_0^\Lambda \frac{l^2 dl}{2\pi^2} U_\alpha(E, l)G_{\alpha\beta}(E, l)H_\beta(s), \end{aligned} \quad (10)$$

where p and \bar{p} are the momenta of the final state D^0 and \bar{D}^0 in the $D\bar{D}^*$ c.m. frame, respectively. $F(p)$ and $H(s)$ represent the transition of $D\bar{D}^*$ to $D^0\bar{D}^0\pi^0$ and $J/\psi\pi^+\pi^-$, respectively,

$$\begin{aligned} F_\alpha(p) &= \delta_{\alpha 0} g_{D^*D\pi} G_{D^*0}(p) q_{1\pi}(p), \\ H_\alpha(s) &= \sqrt{2} g_{\rho\pi\pi} v_{\alpha\rho} G_\rho(s) q_{2\pi}(s), \end{aligned} \quad (11)$$

where $q_{1\pi}$ ($q_{2\pi}$) is the momentum of π^0 (π^+) in the rest frame of D^* (ρ^0), $G_{D^*0}(p) \equiv G_{00}(E; p)/(2m_{D^*0})$ is the D^*0 propagator, and $g_{\rho\pi\pi}$ and $g_{D^*D\pi}$ are the coupling constants for the $\rho\pi\pi$ and $D^*D\pi$ vertices, respectively.

NUMERICAL RESULTS

In the BESIII data [20] for the $J/\psi\pi^+\pi^-$ distribution, besides the resonance signal (taken to be from $X(3872)$ in Ref. [44]), there is a smooth background. The same is true for the LHCb data for the same X decay channel [16]. We take the noninterfering backgrounds in the $J/\psi\pi^+\pi^-$ distributions from the experimental analyses and subtract them from the data to obtain the signal distributions. In terms of the production amplitudes of Eq. (10), the expressions for the experimental yields read

$$\begin{aligned} \frac{d\text{Br}[D^0\bar{D}^0\pi^0]}{dE} &= \frac{1}{32\pi^3} \int_0^{p_{\max}} \frac{p dp}{\omega_{D^0}(p)} \int_{\bar{p}_{\min}}^{\bar{p}_{\max}} \frac{\bar{p} d\bar{p}}{\omega_{\bar{D}^0}(\bar{p})} \\ &\quad \times (|\mathcal{A}_{D^0\bar{D}^0\pi^0}(E, p, \bar{p})|^2 + f_{\text{bg}}), \\ \frac{d^2\text{Br}[J/\psi\pi^+\pi^-]}{dE dm_{2\pi}} &= \int d\Phi_{2\pi} \frac{k_{J/\psi}(E, m_{2\pi}) m_{2\pi}}{4\pi^2 E} \end{aligned}$$

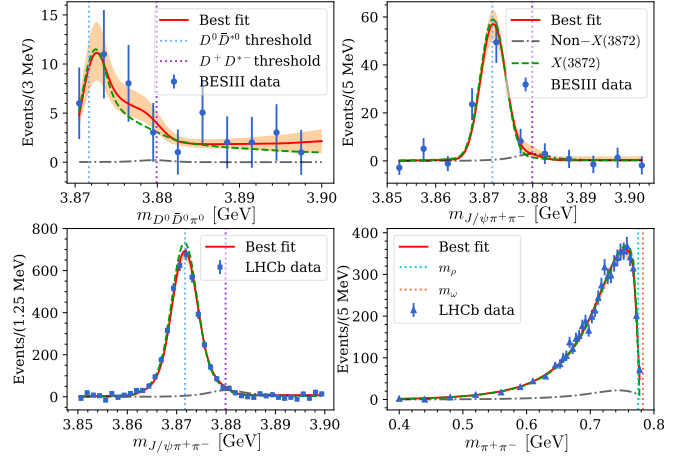


FIG. 1. Best fit of BESIII data on $e^+e^- \rightarrow \gamma(D^0\bar{D}^0\pi^0/J/\psi\pi^+\pi^-)$ [20] (first line) and LHCb data on $B^+ \rightarrow K^+(J/\psi\pi^+\pi^-)$ with $J/\psi\pi^+\pi^-$ distribution from Ref. [16] and $\pi^+\pi^-$ distribution from Ref. [45] (second line). The green dashed and gray dash-dotted curves represent $X(3872)$, described by a Flatté formula as detailed in the Supplemental Materials [46], and the non- $X(3872)$ contributions, respectively.

$$\times |\mathcal{A}_{J/\psi\pi\pi}(E, m_{2\pi}^2, p_+)|^2, \quad (12)$$

where p_{\max} , \bar{p}_{\min} and \bar{p}_{\max} are determined by kinematics, $\omega_{D^0}(p) = \sqrt{m_{D^0}^2 + p^2}$ is the D^0 energy ($\omega_{\bar{D}^0}(\bar{p})$ for \bar{D}^0), $d\Phi_{2\pi}$ is the differential 2-body phase space element of $\pi^+\pi^-$ in the final state, $k_{J/\psi}(E, m_{2\pi})$ is the momentum of J/ψ in the $D\bar{D}^*$ c.m. frame with $m_{2\pi}$ the $\pi^+\pi^-$ invariant mass. We have introduced a non-interfering, constant background term, denoted by f_{bg} , to the $D^0\bar{D}^0\pi^0$ distribution as the background events for this process are not subtracted from the data because of the large uncertainties. In addition, the P_α parameters parametrize the source term and at the same time provide the normalization constants. Since we have two kinds of sources for producing the open-charm $D\bar{D}^*$ pairs, one from e^+e^- annihilations and the other from B decays, the production parameters denoted by P_α^{B} and P_α^{L} for the BESIII and LHCb data, respectively, are different.

In total, there are 9 free parameters to be determined through simultaneously fitting (using MINUIT [47–49]) to the BESIII [20] and LHCb [16, 45] data: P_0^{B} , P_{\pm}^{B} , P_0^{L} , P_{\pm}^{L} , C_{0X} , C_{1X} , a , $u_{0\rho}$, and f_{bg} . The data can be accurately described, with the best fit yielding $\chi^2/\text{dof} = 67.5/87 = 0.78$ for $\Lambda = 1.0 \text{ GeV}$, where “dof” denotes the number of degrees of freedom in the fit. Figure 1 illustrates a comparison of our results with the data, with the orange bands indicating the lineshapes within 1σ statistical uncertainty propagated from the experimental data. Energy resolutions and efficiencies provided in Refs. [16, 20, 45] were included in the fits. Parameter values, the correlation matrix from the best fit and the fitting results for $\Lambda = 0.6 \text{ GeV}$ and 1.4 GeV can be found

in the Supplemental Materials [46].

To include the effect of the additional decay channels of $X(3872)$ in the analysis, we employ the relative branching ratios reported in Refs. [36, 50, 51],³ which lead to an estimate of the contributions from other inelastic channels to the $X(3872)$ width to be $\lesssim 20$ keV. To account for this, we add an imaginary number, C^{inel} , to the potential, which contributes 20 keV to the $X(3872)$ width. Refitting the data shows that all parameters and the real part of the $X(3872)$ pole are within current uncertainties, but the imaginary part of the pole location grows. We include this shift into the uncertainties.

With the parameters from the best fit, the poles of the scattering amplitudes follow from solving Eq. (1) for complex energies. Labeling different Riemann sheets of the coupled-channel scattering amplitudes by the signs of the imaginary parts of momenta for the two channels $D^0\bar{D}^{*0}$ and D^+D^{*-} (i.e., $\text{RS}_{\pm\pm}$ with RS_{++} the physical sheet), we find the $X(3872)$ pole on sheet RS_{++} , located at

$$E_X = (-53_{-24}^{+9} - i 34_{-12}^{+2}) \text{ keV} \quad (13)$$

relative to the nominal $D^0\bar{D}^{*0}$ threshold at 3871.69 MeV. The central value is obtained with $\Lambda=1.0$ GeV, the uncertainties, added in quadrature, contain the statistical uncertainty inherited from the experimental data, the systematic uncertainty from varying Λ from 0.6 GeV to 1.4 GeV, and the above mentioned effect from the additional inelastic channels. The real part is consistent with the ones obtained in the analyses performed by LHCb [19] and BESIII [20] using the generalized Flatté parameterization of Ref. [52], but with a significantly reduced uncertainty. In particular, we establish a (quasi-)bound state nature of $X(3872)$ with a significance of 6σ for the first time. The imaginary part implies that the partial decay width of $X(3872)$ into open-charm channels $D^0\bar{D}^0\pi^0 + D\bar{D}\gamma$ (thus $D^0\bar{D}^{*0}$ is already included) and hidden-charm channels is 69_{-4}^{+24} keV. The former is dominant, contributing about 54 keV, which agree to the total decay width of D^{*0} [53, 54], and the latter contributes 15_{-4}^{+24} keV. In addition, we find $\Gamma_{X(3872)\rightarrow J/\psi 2\pi} = 4.4_{-0.9}^{+1.7}$ keV and $\Gamma_{X(3872)\rightarrow J/\psi 3\pi} = 10.5_{-2.4}^{+4.9}$ keV, and thus

$$\frac{\text{Br}(X(3872) \rightarrow J/\psi 3\pi)}{\text{Br}(X(3872) \rightarrow J/\psi 2\pi)} = 2.4(6). \quad (14)$$

It is important to stress that there is another pole on sheet RS_{+-} , located at

$$(1.6_{-0.9}^{+0.7} + i 1.4_{-0.6}^{+0.3}) \text{ MeV} \quad (15)$$

³ Although the W_{c1} contribution was not considered there, we expect them to provide reasonable estimates.

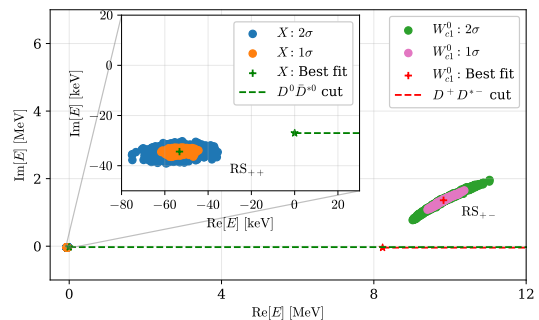


FIG. 2. Pole positions of $X(3872)$ and W_{c1}^0 , relative to the $D^0\bar{D}^{*0}$ threshold, from our analysis with 1σ and 2σ statistical uncertainties.

relative to the nominal D^+D^{*-} threshold at 3879.92 MeV. It corresponds to the isovector W_{c1}^0 state predicted recently [25]. In contrast to the $X(3872)$ pole, this one is not directly connected to the physical region. It manifests itself as a cusp at the D^+D^{*-} threshold [25]. Both poles are presented in Fig. 2.

To quantify the impact of W_{c1}^0 , we remove the $X(3872)$ contributions, represented by the green dashed curves from the $D^0\bar{D}^0\pi^0$ and $J/\psi\pi^+\pi^-$ distributions, from the full amplitudes, as shown by the gray dash-dotted curves in Fig. 1. The $X(3872)$ is here described by the Flatté parameterization with parameters adjusted to reproduce the $X(3872)$ pole position and residues to the elastic channels following the recipe of Ref. [31]—for details see the Supplemental Materials [46]. The absence of a distinct structure of W_{c1}^0 is attributed to the dominance of T_{00} , which has a dip instead of a peak at the D^+D^{*-} threshold [25], resulting from the higher production rate of the neutral channel in both reactions, i.e., $|P_0| > |P_{\pm}|$ —the best fit values are $P_{\pm}^B/P_0^B = 0.57(46)$ and $P_{\pm}^L/P_0^L = 0.45(5)$. The reason for this pattern is that in e^+e^- annihilations, $X(3872)$ is produced dominantly through the radiative decay of $Y(4230)$ [44, 55], which has large coupling to $D\bar{D}_1$ in S -wave [56, 57] and the radiative decay of $D_1^0 \rightarrow D^{*0}\gamma$ is significantly larger than that of $D_1^+ \rightarrow D^{*+}\gamma$ [58, 59]. For the B^+ decays, one finds experimentally $\text{Br}(B^+ \rightarrow D^0\bar{D}^{*0}K^+) > \text{Br}(B^+ \rightarrow D^+D^{*-}K^+)$ [60, 61].

In contrast, in B^0 decays the branching ratio to $K^0D^+D^{*-}$ is six times that of $K^0D^0\bar{D}^{*0}$ [61]. Therefore, we expect $|P_{\pm}| > |P_0|$ for the analogous B^0 decays, and thus the signal of W_{c1}^0 in B^0 decays should be more pronounced than that in the B^+ decays. Indeed, by fixing $P_{\pm}/P_0 = 2$, reasonable for B^0 decays, the predicted lineshapes exhibit this feature, as shown in Fig. 3. For comparison we also show the Belle data for $B^0 \rightarrow K^0D^0\bar{D}^0\pi^0$ [62], which are indeed consistent with a sizable W_{c1}^0 contribution, although current data quality does not allow for a firm conclusion. A similar structure is anticipated in the $D^0\bar{D}^0\gamma$ distribution for $B^0 \rightarrow K^0D^0\bar{D}^0\gamma$. We expect that the W_{c1}^0 -induced peak

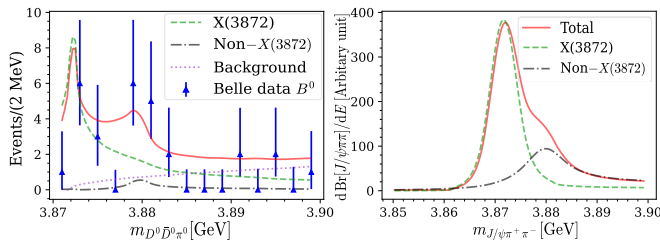


FIG. 3. Predicted $D^0 \bar{D}^0 \pi^0$ (left), in comparison with the Belle data for $B^0 \rightarrow K^0 D^0 \bar{D}^0 \pi^0$ [62], and $J/\psi \pi^+ \pi^-$ (right) distributions using $P_{\pm}/P_0 = 2$. Convolutions with the Belle [62] and LHCb [16] energy resolutions are considered in the left and right panels, respectively.

can be unambiguously identified with the full Belle II statistics. The predicted nontrivial right shoulder of the $J/\psi \pi^+ \pi^-$ distribution in the right panel of Fig. 3 can be checked through $B^0 \rightarrow K^0 J/\psi \pi^+ \pi^-$ at both LHCb and Belle II. Furthermore, one can also detect the charged partners of W_{c1}^0 in the charged channels, where a threshold cusp should appear at the $D^+ \bar{D}^{*0}$ threshold, as discussed in Ref. [25]. However, the neutral channel has the advantage that the signal gets enhanced by the interference with the signal from $X(3872)$.

We also notice the conflict of more than 5σ for $\Gamma_{X(3872) \rightarrow J/\psi \gamma} / \Gamma_{X(3872) \rightarrow \psi(2S) \gamma}$ between the measurements by LHCb in $B^+ \rightarrow K^+ X(3872)$ [51] and by BESIII in $e^+ e^- \rightarrow \gamma X(3872)$ [36]. This conflict may be resolved by considering that the observed signals contain different W_{c1} contributions in these two cases, arising from the different production rates of $D^0 \bar{D}^{*0}$ and $D^+ D^{*-}$ in B^+ decays and $e^+ e^-$ annihilations.

Another important property related to the nature of $X(3872)$ is the significant isospin breaking in its decays, quantified by the ratio of its couplings to $J/\psi \rho^0$ and $J/\psi \omega$, defined as $R_X \equiv |g_{X J/\psi \rho} / g_{X J/\psi \omega}|$ [37, 63, 64]. While there have been determinations of R_X [41, 45, 65, 66], none of them so far has considered that the data contain W_{c1}^0 contributions. In the formalism presented here, the isospin breaking parameter R_X is given by the ratio of the production amplitudes of $J/\psi \rho$ and $J/\psi \omega$ from a given source at the $X(3872)$ mass. Explicitly, evaluated at the pole, we have

$$R_X = \left| \frac{\int_0^\Lambda l^2 dl U_\alpha(E_X, l) G_{\alpha\beta}(E_X, l) u_{\beta\rho}}{\int_0^\Lambda l^2 dl U_\alpha(E_X, l) G_{\alpha\beta}(E_X, l) u_{\beta\omega}} \right| = 0.28(4), \quad (16)$$

which is slightly larger than the value 0.26(3) obtained without the W_{c1}^0 contribution [41].

The low-energy parameters of the $D^0 \bar{D}^{*0}$ system, specifically the S -wave scattering length a_0 and effective range r_0 , are crucial for determining the compositeness of $X(3872)$ [67]. However, the values extracted in Refs. [19, 20] have large uncertainties. Furthermore, these results require a correction for isospin-breaking effects for r_0 due to channel coupling, leading to a cor-

rected r'_0 [68]. After considering these and expanding T_{00} around the $D^0 \bar{D}^{*0}$ complex threshold [68, 69], we find that $a_0 = (-19.0^{+2.6}_{-1.8} + i 1.7^{+1.7}_{-0.4})$ fm and $r'_0 = -0.1^{+0.4}_{-0.2}$ fm. Thus the current data are consistent only with a very small or even positive effective range, providing strong support for a molecular nature of $X(3872)$ in line with the reasoning of Refs. [68, 70, 71]. Quantitatively, the compositeness of $X(3872)$ can be estimated to be [72]

$$\bar{X}_A = \left(1 + 2 \left| \frac{r'_0}{\text{Re } a_0} \right| \right)^{-\frac{1}{2}} > 0.99, \quad (17)$$

consistent with unity.

CONCLUSION

We have determined the $X(3872)$ properties with unprecedented accuracy by fitting a large set of experimental data with an improved formalism. More precisely, we demonstrate the data are consistent with $X(3872)$ emerging as a molecular state from $D^0 \bar{D}^{*0}$ and $D^+ D^{*-}$ coupled-channel interactions. The inelastic coupled channels $J/\psi \rho$ and $J/\psi \omega$ are taken into account explicitly. The $X(3872)$ is determined to be a (quasi-)bound state with a significance of 6σ , with a pole located at $(-53^{+9}_{-24} - i 34^{+2}_{-12})$ keV relative to the $D^0 \bar{D}^{*0}$ threshold. The isospin breaking ratio of its decays into $J/\psi \rho^0$ and $J/\psi \omega$ is determined as $R_X = 0.28(4)$.

We have also determined the pole of the isospin-vector partner of $X(3872)$, W_{c1}^0 predicted in [25], to be at $(1.6^{+0.7}_{-0.9} + i 1.4^{+0.3}_{-0.6})$ MeV relative to the $D^+ D^{*-}$ threshold on an unphysical Riemann sheet.

The W_{c1}^0 leads to very mild distortions of the $D^0 \bar{D}^0 \pi^0$ and $J/\psi \pi^+ \pi^-$ distributions from the $X(3872)$ line shapes in both $e^+ e^-$ collisions and B^+ decays. Its signal should be more clearly visible in reactions where $D^+ D^{*-}$ is more frequently produced than $D^0 \bar{D}^{*0}$, such as $B^0 \rightarrow K^0 D \bar{D}^*$ decays, which can be verified at Belle II and LHCb.

With the confirmation of W_{c1} , an SU(3) flavor multiplet structure for hidden-charm hadronic molecules is emerging. Unlike compact tetraquark models, where all states are bound states of quarks and antiquarks, the molecular picture allows for a richer spectrum of states, including both bound and virtual states, with the latter showing up as threshold cusps. The $X(3872)$ and W_{c1} are prime examples of such a spectrum. The situation reminds of the two-nucleon systems, where the deuteron is an isoscalar proton-neutron bound state and a virtual pole exists in the isovector sector. More similar structures are expected to be found in the future. Investigating these states will provide deeper insights not only into the hadron spectrum but also fundamental questions, such as why thousands of atomic nuclei exist while no evidence for compact multi-quark states with $3n$ ($n \geq 2$)

quarks has been found, ultimately shedding light on the nature of the inner workings of the strong force.

We are grateful to Vanya Belyaev, Ji-Bo He, Xiao-Yu Li, Tomasz Skwarnicki, Chang-Zheng Yuan and Zhen-Hua Zhang for fruitful discussions. This work is supported in part by the National Key R&D Program of China under Grant No. 2023YFA1606703; by the National Natural Science Foundation of China (NSFC) under Grants No. 12125507, No. 12361141819, and No. 12047503; and by the Chinese Academy of Sciences (CAS) under Grants No. YSBR-101. In addition, U.-G.M. and C.H. thank the CAS President's International Fellowship Initiative (PIFI) under Grant Nos. 2025PD0022 and 2025PD0087, respectively, for partial support.

* teng@hiskp.uni-bonn.de

† xiangkun@hiskp.uni-bonn.de

‡ Corresponding author: fkguo@itp.ac.cn

§ c.hanhart@fz-juelich.de

¶ meissner@hiskp.uni-bonn.de

- [1] S. K. Choi *et al.* (Belle), Observation of a narrow charmonium-like state in exclusive $B^\pm \rightarrow K^\pm \pi^+ \pi^- J/\psi$ decays, *Phys. Rev. Lett.* **91**, 262001 (2003), [arXiv:hep-ex/0309032](https://arxiv.org/abs/hep-ex/0309032).
- [2] S. Navas and Others (Particle Data Group), Review of Particle Physics, *Phys. Rev. D* **110**, 030001 (2024).
- [3] R. Aaij *et al.* (LHCb), Determination of the $X(3872)$ meson quantum numbers, *Phys. Rev. Lett.* **110**, 222001 (2013), [arXiv:1302.6269](https://arxiv.org/abs/1302.6269) [hep-ex].
- [4] R. Aaij *et al.* (LHCb), Quantum numbers of the $X(3872)$ state and orbital angular momentum in its $\rho^0 J\psi$ decay, *Phys. Rev. D* **92**, 011102 (2015), [arXiv:1504.06339](https://arxiv.org/abs/1504.06339) [hep-ex].
- [5] A. Hosaka, T. Iijima, K. Miyabayashi, Y. Sakai, and S. Yasui, Exotic hadrons with heavy flavors: X , Y , Z , and related states, *PTEP* **2016**, 062C01 (2016), [arXiv:1603.09229](https://arxiv.org/abs/1603.09229) [hep-ph].
- [6] A. Esposito, A. Pilloni, and A. D. Polosa, Multiquark Resonances, *Phys. Rept.* **668**, 1 (2017), [arXiv:1611.07920](https://arxiv.org/abs/1611.07920) [hep-ph].
- [7] F.-K. Guo, C. Hanhart, U.-G. Meißner, Q. Wang, Q. Zhao, and B.-S. Zou, Hadronic molecules, *Rev. Mod. Phys.* **90**, 015004 (2018), [arxiv:1705.00141](https://arxiv.org/abs/1705.00141) [hep-ph].
- [8] S. L. Olsen, T. Skwarnicki, and D. Zieminska, Nonstandard heavy mesons and baryons: Experimental evidence, *Rev. Mod. Phys.* **90**, 015003 (2018), [arXiv:1708.04012](https://arxiv.org/abs/1708.04012) [hep-ph].
- [9] M. Karliner, J. L. Rosner, and T. Skwarnicki, Multiquark States, *Ann. Rev. Nucl. Part. Sci.* **68**, 17 (2018), [arXiv:1711.10626](https://arxiv.org/abs/1711.10626) [hep-ph].
- [10] Y. S. Kalashnikova and A. V. Nefediev, $X(3872)$ in the molecular model, *Phys. Usp.* **62**, 568 (2019), [arXiv:1811.01324](https://arxiv.org/abs/1811.01324) [hep-ph].
- [11] N. Brambilla, S. Eidelman, C. Hanhart, A. Nefediev, C.-P. Shen, C. E. Thomas, A. Vairo, and C.-Z. Yuan, The XYZ states: experimental and theoretical status and perspectives, *Phys. Rept.* **873**, 1 (2020), [arXiv:1907.07583](https://arxiv.org/abs/1907.07583) [hep-ex].
- [12] L. Meng, B. Wang, G.-J. Wang, and S.-L. Zhu, Chiral perturbation theory for heavy hadrons and chiral effective field theory for heavy hadronic molecules, *Phys. Rept.* **1019**, 1 (2023), [arXiv:2204.08716](https://arxiv.org/abs/2204.08716) [hep-ph].
- [13] M.-Z. Liu, Y.-W. Pan, Z.-W. Liu, T.-W. Wu, J.-X. Lu, and L.-S. Geng, Three ways to decipher the nature of exotic hadrons: Multiplets, three-body hadronic molecules, and correlation functions, *Phys. Rept.* **1108**, 1 (2025), [arXiv:2404.06399](https://arxiv.org/abs/2404.06399) [hep-ph].
- [14] J. Chen, F.-K. Guo, Y.-G. Ma, C.-P. Shen, Q. Shou, Q. Wang, J.-J. Wu, and B.-S. Zou, Production of exotic hadrons in pp and nuclear collisions, *Nucl. Sci. Tech.* **10.1007/s41365-025-01664-w** (2025), [arXiv:2411.18257](https://arxiv.org/abs/2411.18257) [hep-ph].
- [15] M. Ablikim *et al.* (BESIII), Observation of a New $X(3872)$ Production Process $e^+e^- \rightarrow \omega X(3872)$, *Phys. Rev. Lett.* **130**, 151904 (2023), [arXiv:2212.07291](https://arxiv.org/abs/2212.07291) [hep-ex].
- [16] R. Aaij *et al.* (LHCb), Study of the $\psi_2(3823)$ and $\chi_{c1}(3872)$ states in $B^+ \rightarrow (J/\psi \pi^+ \pi^-) K^+$ decays, *JHEP* **08**, 123, [arXiv:2005.13422](https://arxiv.org/abs/2005.13422) [hep-ex].
- [17] T. Aaltonen *et al.* (CDF), Precision Measurement of the $X(3872)$ Mass in $J/\psi \pi^+ \pi^-$ Decays, *Phys. Rev. Lett.* **103**, 152001 (2009), [arXiv:0906.5218](https://arxiv.org/abs/0906.5218) [hep-ex].
- [18] C. Hanhart, Y. S. Kalashnikova, A. E. Kudryavtsev, and A. V. Nefediev, Reconciling the $X(3872)$ with the near-threshold enhancement in the $D^0 \bar{D}^{*0}$ final state, *Phys. Rev. D* **76**, 034007 (2007), [arXiv:0704.0605](https://arxiv.org/abs/0704.0605) [hep-ph].
- [19] R. Aaij *et al.* (LHCb), Study of the lineshape of the $\chi_{c1}(3872)$ state, *Phys. Rev. D* **102**, 092005 (2020), [arXiv:2005.13419](https://arxiv.org/abs/2005.13419) [hep-ex].
- [20] M. Ablikim *et al.* (BESIII), Coupled-Channel Analysis of the $\chi_{c1}(3872)$ Line Shape with BESIII Data, *Phys. Rev. Lett.* **132**, 151903 (2024), [arXiv:2309.01502](https://arxiv.org/abs/2309.01502) [hep-ex].
- [21] V. Baru, A. A. Filin, C. Hanhart, Y. S. Kalashnikova, A. E. Kudryavtsev, and A. V. Nefediev, Three-body $D\bar{D}\pi$ dynamics for the $X(3872)$, *Phys. Rev. D* **84**, 074029 (2011), [arXiv:1108.5644](https://arxiv.org/abs/1108.5644) [hep-ph].
- [22] M.-L. Du, V. Baru, X.-K. Dong, A. Filin, F.-K. Guo, C. Hanhart, A. Nefediev, J. Nieves, and Q. Wang, Coupled-channel approach to T_{cc}^+ including three-body effects, *Phys. Rev. D* **105**, 014024 (2022), [arXiv:2110.13765](https://arxiv.org/abs/2110.13765) [hep-ph].
- [23] T. Ji, X.-K. Dong, F.-K. Guo, and B.-S. Zou, Prediction of a Narrow Exotic Hadronic State with Quantum Numbers $J^{PC} = 0^{--}$, *Phys. Rev. Lett.* **129**, 102002 (2022), [arXiv:2205.10994](https://arxiv.org/abs/2205.10994) [hep-ph].
- [24] X.-K. Dong, T. Ji, F.-K. Guo, U.-G. Meißner, and B.-S. Zou, Hints of the $J^{PC} = 0^{--}$ and $1^{--} K^* \bar{K}_1(1270)$ molecules in the $J/\psi \rightarrow \phi \eta \eta'$ decay, *Phys. Lett. B* **853**, 138646 (2024), [arXiv:2402.02903](https://arxiv.org/abs/2402.02903) [hep-ph].
- [25] Z.-H. Zhang, T. Ji, X.-K. Dong, F.-K. Guo, C. Hanhart, U.-G. Meißner, and A. Rusetsky, Predicting isovector charmonium-like states from $X(3872)$ properties, *JHEP* **08**, 130, [arXiv:2404.11215](https://arxiv.org/abs/2404.11215) [hep-ph].
- [26] T. D. Cohen, B. A. Gelman, and U. van Kolck, An effective field theory for coupled channel scattering, *Phys. Lett. B* **588**, 57 (2004), [arXiv:nuel-th/0402054](https://arxiv.org/abs/nuel-th/0402054).
- [27] E. Braaten and M. Kusunoki, Factorization in the production and decay of the $X(3872)$, *Phys. Rev. D* **72**, 014012 (2005), [arXiv:hep-ph/0506087](https://arxiv.org/abs/hep-ph/0506087).
- [28] X.-K. Dong, F.-K. Guo, and B.-S. Zou, Explain-

- ing the many threshold structures in the heavy-quark hadron spectrum, *Phys. Rev. Lett.* **126**, 152001 (2021), [arXiv:2011.14517 \[hep-ph\]](#).
- [29] Z.-H. Zhang and F.-K. Guo, Classification of Coupled-Channel Near-Threshold Structures, (2024), [arXiv:2407.10620 \[hep-ph\]](#).
- [30] K. Sone and T. Hyodo, General amplitude of near-threshold hadron scattering for exotic hadrons, (2024), [arXiv:2405.08436 \[hep-ph\]](#).
- [31] L. A. Heuser, G. Chanturia, F. K. Guo, C. Hanhart, M. Hoferichter, and B. Kubis, From pole parameters to line shapes and branching ratios, *Eur. Phys. J. C* **84**, 599 (2024), [arXiv:2403.15539 \[hep-ph\]](#).
- [32] M. Sadl, S. Collins, Z.-H. Guo, M. Padmanath, S. Prelovsek, and L.-W. Yan, Charmoniumlike channels 1^+ with isospin 1 from lattice and effective field theory, (2024), [arXiv:2406.09842 \[hep-lat\]](#).
- [33] T. Aushev *et al.* (Belle), Study of the $B \rightarrow X(3872)(D^{*0}\bar{D}^0)K$ decay, *Phys. Rev. D* **81**, 031103 (2010), [arXiv:0810.0358 \[hep-ex\]](#).
- [34] C. Li and C.-Z. Yuan, Determination of the absolute branching fractions of $X(3872)$ decays, *Phys. Rev. D* **100**, 094003 (2019), [arXiv:1907.09149 \[hep-ex\]](#).
- [35] E. Braaten, L.-P. He, and K. Inles, Branching Fractions of the $X(3872)$, (2019), [arXiv:1908.02807 \[hep-ph\]](#).
- [36] M. Ablikim *et al.* (BESIII), Study of Open-Charmed Decays and Radiative Transitions of the $X(3872)$, *Phys. Rev. Lett.* **124**, 242001 (2020), [arXiv:2001.01156 \[hep-ex\]](#).
- [37] C. Hidalgo-Duque, J. Nieves, and M. P. Valderrama, Light flavor and heavy quark spin symmetry in heavy meson molecules, *Phys. Rev. D* **87**, 076006 (2013), [arXiv:1210.5431 \[hep-ph\]](#).
- [38] C. Hanhart, Y. S. Kalashnikova, P. Matuschek, R. V. Mizuk, A. V. Nefediev, and Q. Wang, Practical Parametrization for Line Shapes of Near-Threshold States, *Phys. Rev. Lett.* **115**, 202001 (2015), [arXiv:1507.00382 \[hep-ph\]](#).
- [39] F.-K. Guo, C. Hanhart, Yu. S. Kalashnikova, P. Matuschek, R. V. Mizuk, A. V. Nefediev, Q. Wang, and J. L. Wynen, Interplay of quark and meson degrees of freedom in near-threshold states: A practical parametrization for line shapes, *Phys. Rev. D* **93**, 074031 (2016), [arXiv:1602.00940 \[hep-ph\]](#).
- [40] R. Omnès, On the Solution of certain singular integral equations of quantum field theory, *Nuovo Cim.* **8**, 316 (1958).
- [41] J. M. Dias, T. Ji, X.-K. Dong, F.-K. Guo, C. Hanhart, U.-G. Meißner, Y. Zhang, and Z.-H. Zhang, Dispersive analysis of the isospin breaking in the $X(3872) \rightarrow J/\psi\pi^+\pi^-$ and $X(3872) \rightarrow J/\psi\pi^+\pi^0\pi^-$ decays, *Phys. Rev. D* **111**, 014031 (2025), [arXiv:2409.13245 \[hep-ph\]](#).
- [42] F. Stollenwerk, C. Hanhart, A. Kupsc, U.-G. Meißner, and A. Wirzba, Model-independent approach to $\eta \rightarrow \pi^+\pi^-\gamma$ and $\eta' \rightarrow \pi^+\pi^-\gamma$, *Phys. Lett. B* **707**, 184 (2012), [arXiv:1108.2419 \[nucl-th\]](#).
- [43] C. Hanhart, A. Kupsc, U.-G. Meißner, F. Stollenwerk, and A. Wirzba, Dispersive analysis for $\eta \rightarrow \gamma\gamma^*$, *Eur. Phys. J. C* **73**, 2668 (2013), [Erratum: *Eur. Phys. J. C* **75**, 242 (2015)], [arXiv:1307.5654 \[hep-ph\]](#).
- [44] M. Ablikim *et al.* (BESIII), Observation of $e^+e^- \rightarrow \gamma X(3872)$ at BESIII, *Phys. Rev. Lett.* **112**, 092001 (2014), [arXiv:1310.4101 \[hep-ex\]](#).
- [45] R. Aaij *et al.* (LHCb), Observation of sizeable ω contribution to $\chi_{c1}(3872) \rightarrow \pi^+\pi^-J/\psi$ decays, *Phys. Rev. D* **108**, L011103 (2023), [arXiv:2204.12597 \[hep-ex\]](#).
- [46] See the Supplemental Materials for the best fit parameter values, lineshapes with different cutoffs, and details of the $X(3872)$ pole subtraction.
- [47] F. James and M. Roos, Minuit: A System for Function Minimization and Analysis of the Parameter Errors and Correlations, *Comput. Phys. Commun.* **10**, 343 (1975).
- [48] H. Dembinski *et al.* (iminuit team), iminuit: A python interface to minuit, <https://github.com/scikit-hep/iminuit>.
- [49] F.-K. Guo and Y. Zhang, Iminuit.jl: A julia wrapper of iminuit, <https://github.com/fkguo/IMinuit.jl>.
- [50] M. Ablikim *et al.* (BESIII), Observation of the decay $X(3872) \rightarrow \pi^0\chi_{c1}(1P)$, *Phys. Rev. Lett.* **122**, 202001 (2019), [arXiv:1901.03992 \[hep-ex\]](#).
- [51] I. Bezshyiko *et al.* (LHCb), Probing the nature of the $\chi_{c1}(3872)$ state using radiative decays, *JHEP* **11**, 121, [arXiv:2406.17006 \[hep-ex\]](#).
- [52] C. Hanhart, Yu. S. Kalashnikova, and A. V. Nefediev, Lineshapes for composite particles with unstable constituents, *Phys. Rev. D* **81**, 094028 (2010), [arXiv:1002.4097 \[hep-ph\]](#).
- [53] J. L. Rosner, Hadronic and radiative D^* widths, *Phys. Rev. D* **88**, 034034 (2013), [arXiv:1307.2550 \[hep-ph\]](#).
- [54] F.-K. Guo, Novel method for precisely measuring the $X(3872)$ mass, *Phys. Rev. Lett.* **122**, 202002 (2019), [arXiv:1902.11221 \[hep-ph\]](#).
- [55] F.-K. Guo, C. Hanhart, U.-G. Meißner, Q. Wang, and Q. Zhao, Production of the $X(3872)$ in charmonia radiative decays, *Phys. Lett. B* **725**, 127 (2013), [arXiv:1306.3096 \[hep-ph\]](#).
- [56] Q. Wang, C. Hanhart, and Q. Zhao, Decoding the riddle of $Y(4260)$ and $Z_c(3900)$, *Phys. Rev. Lett.* **111**, 132003 (2013), [arXiv:1303.6355 \[hep-ph\]](#).
- [57] L. von Detten, V. Baru, C. Hanhart, Q. Wang, D. Winney, and Q. Zhao, How many vector charmoniumlike states lie in the mass range 4.2–4.35 GeV?, *Phys. Rev. D* **109**, 116002 (2024), [arXiv:2402.03057 \[hep-ph\]](#).
- [58] J. G. Körner, D. Pirjol, and K. Schilcher, Radiative decays of the p -wave charmed mesons, *Phys. Rev. D* **47**, 3955 (1993), [arXiv:hep-ph/9212220](#).
- [59] Fayyazuddin and O. Mobarek, Radiative decay of $D_2^*(2460)$ and $D_1(2420)$, *Phys. Rev. D* **50**, 2329 (1994).
- [60] B. Aubert *et al.* (BaBar), Measurement of the branching fractions for the exclusive decays of B^0 and B^+ to $\bar{D}^{(*)}D^{(*)}K$, *Phys. Rev. D* **68**, 092001 (2003), [arXiv:hep-ex/0305003](#).
- [61] P. del Amo Sanchez *et al.* (BaBar), Measurement of the $B \rightarrow \bar{D}^{(*)}D^{(*)}K$ branching fractions, *Phys. Rev. D* **83**, 032004 (2011), [arXiv:1011.3929 \[hep-ex\]](#).
- [62] H. Hirata *et al.* (Belle), Study of the lineshape of $X(3872)$ using B decays to $D^0\bar{D}^{*0}K$, *Phys. Rev. D* **107**, 112011 (2023), [arXiv:2302.02127 \[hep-ex\]](#).
- [63] M. Suzuki, The $X(3872)$ boson: Molecule or charmonium, *Phys. Rev. D* **72**, 114013 (2005), [arXiv:hep-ph/0508258](#).
- [64] D. Gamermann, J. Nieves, E. Oset, and E. Ruiz Arriola, Couplings in coupled channels versus wave functions: application to the $X(3872)$ resonance, *Phys. Rev. D* **81**, 014029 (2010), [arXiv:0911.4407 \[hep-ph\]](#).
- [65] C. Hanhart, Y. S. Kalashnikova, A. E. Kudryavtsev, and A. V. Nefediev, Remarks on the quantum numbers of

- $X(3872)$ from the invariant mass distributions of the $\rho J/\psi$ and $\omega J/\psi$ final states, *Phys. Rev. D* **85**, 011501 (2012), arXiv:1111.6241 [hep-ph].
- [66] H.-N. Wang, Q. Wang, and J.-J. Xie, Theoretical study on the contributions of ω meson to the $X(3872) \rightarrow J/\psi\pi^+\pi^-$ and $J/\psi\pi^+\pi^-\pi^0$ decays, *Phys. Rev. D* **106**, 056022 (2022), arXiv:2206.14456 [hep-ph].
- [67] S. Weinberg, Evidence That the Deuteron Is Not an Elementary Particle, *Phys. Rev.* **137**, B672 (1965).
- [68] V. Baru, X.-K. Dong, M.-L. Du, A. Filin, F.-K. Guo, C. Hanhart, A. Nefediev, J. Nieves, and Q. Wang, Effective range expansion for narrow near-threshold resonances, *Phys. Lett. B* **833**, 137290 (2022), arXiv:2110.07484 [hep-ph].
- [69] E. Braaten and J. Stapleton, Analysis of $J/\psi\pi^+\pi^-$ and $D^0\bar{D}^0\pi^0$ decays of the $X(3872)$, *Phys. Rev. D* **81**, 014019 (2010), arXiv:0907.3167 [hep-ph].
- [70] A. Esposito, L. Maiani, A. Pilloni, A. D. Polosa, and V. Riquer, From the line shape of the $X(3872)$ to its structure, *Phys. Rev. D* **105**, L031503 (2022), arXiv:2108.11413 [hep-ph].
- [71] Y. Li, F.-K. Guo, J.-Y. Pang, and J.-J. Wu, Generalization of Weinberg's compositeness relations, *Phys. Rev. D* **105**, L071502 (2022), arXiv:2110.02766 [hep-ph].
- [72] I. Matuschek, V. Baru, F.-K. Guo, and C. Hanhart, On the nature of near-threshold bound and virtual states, *Eur. Phys. J. A* **57**, 101 (2021), arXiv:2007.05329 [hep-ph].

Supplemental Materials

Diagrams for $D^0\bar{D}^0\pi^0$ production

Diagram representations of the $D^0\bar{D}^0\pi^0$ and $J/\psi\pi^+\pi^-$ productions in Eqs. (9 and 10) are shown in Figs. 4 and 5.

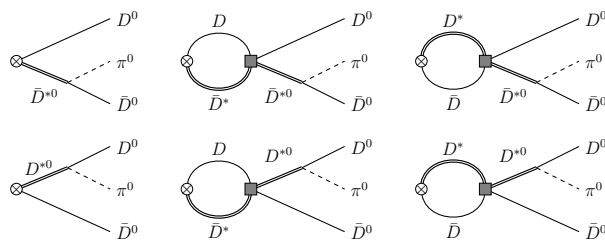


FIG. 4. Diagrams for $D^0\bar{D}^0\pi^0$ production. The gray square represents the DD^* scattering in $J^{PC} = 1^{++}$ channels and \otimes represents the production of DD^* from the given 1^{++} source.

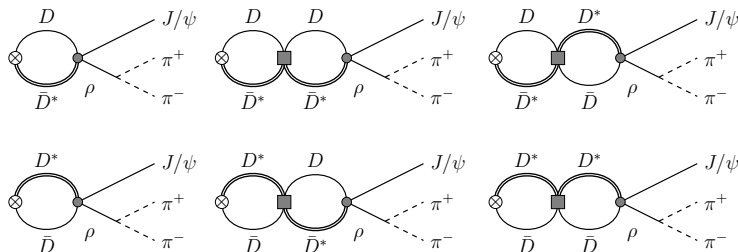


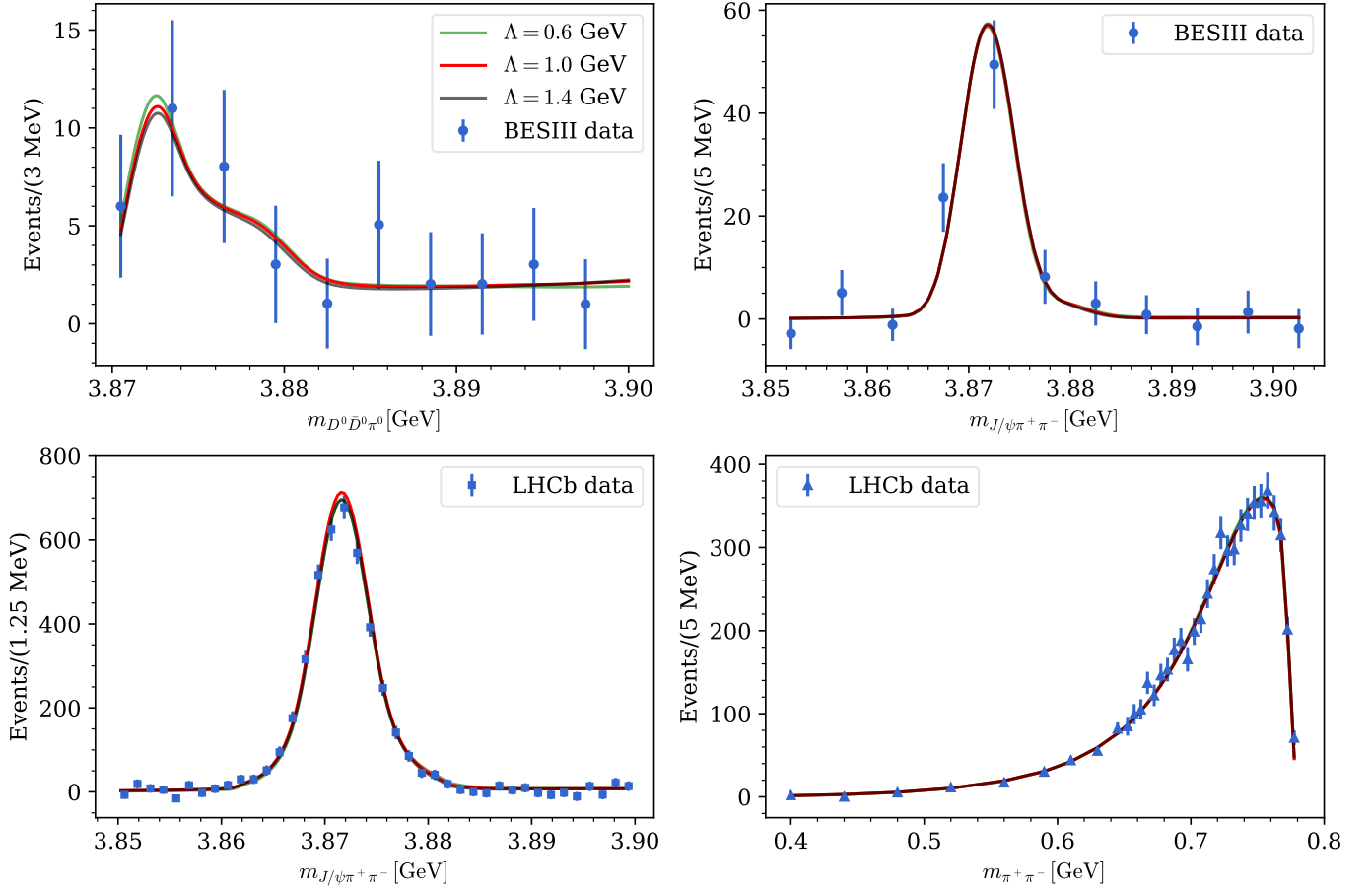
FIG. 5. Similar with Fig. 4 but for the $J/\psi\pi^+\pi^-$ production. The gray circle stands for the elastic-inelastic transition with ρ - ω mixing included.

Parameter values from the best fit and lineshapes for different Λ

The parameter values and the correlation matrix from the best fit are listed in Table I. We show the lineshapes of the best fits with different values for the cutoff parameter Λ in Fig. 6. The best fits have similar quality and the difference in lineshapes between different Λ values is almost invisible as it should be the case for a properly renormalised effective field theory.

TABLE I. The parameter values for $\Lambda = 0.6, 1.0,$ and 1.4 GeV and the correlation matrix for $\Lambda = 1.0$ GeV from the best fit.

Parameters	$\Lambda = 0.6$ GeV	$\Lambda = 1.0$ GeV	$\Lambda = 1.4$ GeV	Correlation matrix ($\Lambda = 1.0$ GeV)								
$P_0^B/10^3$ [$\text{GeV}^{-3/2}$]	4.82 ± 1.05	2.71 ± 0.78	1.88 ± 0.51	1.00								
P_{\pm}^B/P_0^B	0.46 ± 0.39	0.57 ± 0.46	0.64 ± 0.50	-0.82	1.00							
$P_0^L/10^3$ [$\text{GeV}^{-3/2}$]	8.95 ± 1.30	5.14 ± 1.01	3.61 ± 0.56	0.76	-0.31	1.00						
P_{\pm}^L/P_0^L	0.40 ± 0.04	0.45 ± 0.05	0.48 ± 0.05	-0.09	0.06	-0.16	1.00					
C_{0X} [GeV^{-2}]	-10.79 ± 0.08	-2.97 ± 0.05	-0.05 ± 0.02	0.31	-0.17	0.36	-0.31	1.00				
C_{1X} [GeV^{-2}]	-15.82 ± 0.37	-10.71 ± 0.28	-8.39 ± 0.16	-0.02	0.04	0.02	0.23	-0.89	1.00			
f_{bg} [MeV^{-3}]	18.8 ± 59.8	32.8 ± 60.7	39.7 ± 58.2	-0.34	0.12	-0.41	0.04	-0.17	0.02	1.00		
a [GeV^{-2}]	1.05 ± 0.28	0.85 ± 0.34	0.82 ± 0.35	0.06	-0.06	0.04	-0.23	0.72	-0.79	-0.04	1.00	
$u_{\pm\rho}$ [GeV^{-2}]	-1.34 ± 0.24	-0.87 ± 0.26	-0.64 ± 0.19	0.58	-0.25	0.74	-0.16	0.74	-0.58	-0.32	0.63	1.00
χ^2/dof	0.84	0.78	0.76									

FIG. 6. Comparison between the best fitted lineshapes with $\Lambda = 0.6, 1.0,$ and 1.4 GeV.

Extracting the pole terms of $X(3872)$ and W_{c1}^0 with Flatté parameterization

The couplings of the two poles to elastic channels, which can be extracted by $g_\alpha g_\beta = \lim_{E \rightarrow E_{\text{pole}}} (E - E_{\text{pole}}) T_{\alpha\beta}$, read

$$\begin{aligned} g_{X,0} &= (0.26 \pm 0.02) e^{(0.02 \pm 0.01)i} \text{ GeV}^{-\frac{1}{2}}, \\ g_{X,\pm} &= (0.16 \pm 0.01) e^{(0.02 \pm 0.01)i} \text{ GeV}^{-\frac{1}{2}}, \\ g_{W,0} &= (0.40 \pm 0.01) e^{(-1.03 \pm 0.05)i} \text{ GeV}^{-\frac{1}{2}}, \\ g_{W,\pm} &= (0.60 \pm 0.09) e^{(-2.12 \pm 0.02)i} \text{ GeV}^{-\frac{1}{2}}, \end{aligned} \quad (18)$$

where the errors propagated from data and those from varying Λ from 0.6 to 1.4 GeV have been added in quadrature.

To investigate the contributions of the $X(3872)$ and W_{c1}^0 to the event distributions, we use the Flatté parameterization with its real parameters adjusted to reproduce both pole locations and residues [31]

$$T_{\alpha\beta}^{\text{Flatté}} = \frac{1}{4\sqrt{m_{\alpha 1} m_{\alpha 2} m_{\beta 1} m_{\beta 2}}} \frac{\tilde{g}_\alpha \tilde{g}_\beta}{z - \tilde{m}^2 + \tilde{g}_0^2 \Sigma_0(z) + \tilde{g}_\pm^2 \Sigma_\pm(z) + i \tilde{m} \tilde{\Gamma}}, \quad (19)$$

where $\sqrt{z} = E + m_{D^0} + m_{\bar{D}^{*0}}$ is the total energy in c.m. frame,

$$\Sigma_\alpha(z) = \frac{z - z_{\alpha 0}}{\pi} \int_{z_{\text{th}}}^{\infty} \frac{dz'}{(z' - z_{\alpha 0})(z' - z)} \frac{k_\alpha(z')}{8\pi\sqrt{z'}} \quad (20)$$

is the self-energy function of channel- α with $k_\alpha(z)$ the on-shell momentum, once subtracted at $z_{\alpha 0} = (m_{\alpha 1} + m_{\alpha 2})^2$. The bare parameters, \tilde{g}_α , \tilde{m} , and $\tilde{\Gamma}$, are adjusted to reproduce the pole positions and couplings to the $D^0 \bar{D}^{*0}$ and $D^+ D^{*-}$ channels. The prefactor is introduced to correct for the different normalization of the non-relativistic $T_{\alpha\beta}^{\text{Flatté}}$. For $X(3872)$, the parameters are

$$\tilde{g}_0 = 51.7 \text{ GeV}, \quad \tilde{g}_\pm = 31.1 \text{ GeV}, \quad \tilde{m} = 3.675 \text{ GeV}, \quad \tilde{\Gamma} = 5.1 \text{ MeV}. \quad (21)$$

It turns out that for the W_{c1} , we cannot reproduce the pole position and couplings using the analogous Flatté parameterization. Therefore, in this case a background term would need to be introduced as outlined in Ref. [31]. Alternatively, we define $T_{\alpha\beta}^W = T_{\alpha\beta} - T_{\alpha\beta}^{\text{Flatté},X}$ to calculate the W_{c1} contributions. Using the parameters above and replacing $T_{\alpha\beta}$ in Eq. (9) with $T_{\alpha\beta}^{\text{Flatté},X}$ or $T_{\alpha\beta}^W$, we obtain the contributions of $X(3872)$ and W_{c1}^0 to the event distributions, shown as the green dashed and gray dash-dotted curves in Figs. 1 and 3, respectively. We also find that using only the $X(3872)$ pole term from a Laurent expansion of the scattering amplitudes, which takes the form of a fixed width Breit-Wigner function, instead of the Flatté parameterization in Eq. (19), the $X(3872)$ contribution in the $D^0 \bar{D}^0 \pi^0$ final state would be significantly underestimated.

Inelastic potential V_{inel}

The potential for the transitions between elastic and inelastic channels can be parametrized as

$$\begin{aligned} v_{0\rho}(s) &= (1 + as)(u_{0\rho} + u_{0\omega} \epsilon_{\rho\omega} G_\omega(s)), \\ v_{0\omega}(s) &= (1 + as)(u_{0\omega} + u_{0\rho} \epsilon_{\rho\omega} G_\rho(s)), \\ v_{\pm\rho}(s) &= (1 + as)(u_{\pm\rho} + u_{\pm\omega} \epsilon_{\rho\omega} G_\omega(s)), \\ v_{\pm\omega}(s) &= (1 + as)(u_{\pm\omega} + u_{\pm\rho} \epsilon_{\rho\omega} G_\rho(s)), \end{aligned} \quad (22)$$

with s denoting the invariant mass squared of ρ or ω , which have been written in a matrix form in Eq. (7) in the main text. According to the optical theorem, we have

$$\text{Im}[V_{\alpha\beta}^{\text{inel}}(E, s)] = - \sum_{i=\rho,\omega} v_{\alpha i}(s) \rho_i(E, s) \varrho_i(s) v_{\beta i}^*(s). \quad (23)$$

Employing Eq. (8) and dropping terms quadratic in the mixing, these components read explicitly,

$$\begin{aligned}
\text{Im}[V_{00}^{\text{inel}}(E, s)] &= -(1 + as)^2 (|u_{0\rho} + u_{0\omega}\epsilon_{\rho\omega}G_\omega(s)|^2\rho_\rho(E, s)\varrho_\rho(s) + |u_{0\omega} + u_{0\rho}\epsilon_{\rho\omega}G_\rho(s)|^2\rho_\omega(E, s)\varrho_\omega(s)), \\
\text{Im}[V_{0\pm(\pm 0)}^{\text{inel}}(E, s)] &= -(1 + as)^2 (u_{0\rho} + u_{0\omega}\epsilon_{\rho\omega}G_\omega(s))(u_{\pm\rho} + u_{\pm\omega}\epsilon_{\rho\omega}G_\omega^*(s))\rho_\rho(E, s)\varrho_\rho(s) \\
&\quad - (1 + as)^2 (u_{0\omega} + u_{0\rho}\epsilon_{\rho\omega}G_\rho(s))(u_{\pm\omega} + u_{\pm\rho}\epsilon_{\rho\omega}G_\rho^*(s))\rho_\omega(E, s)\varrho_\omega(s) \\
&= -(1 + as)^2 (u_{0\rho}u_{\pm\rho}\rho_\rho(E, s)\varrho_\rho(s) + u_{0\omega}u_{\pm\omega}\rho_\omega(E, s)\varrho_\omega(s)) + \mathcal{O}(\epsilon_{\rho\omega}^2), \\
\text{Im}[V_{\pm\pm}^{\text{inel}}(E, s)] &= -(1 + as)^2 (|u_{\pm\rho} + u_{\pm\omega}\epsilon_{\rho\omega}G_\omega(s)|^2\rho_\rho(E, s)\varrho_\rho(s) + |u_{\pm\omega} + u_{\pm\rho}\epsilon_{\rho\omega}G_\rho(s)|^2\rho_\omega(E, s)\varrho_\omega(s)).
\end{aligned} \tag{24}$$

Then the inelastic potential can be expressed as

$$\text{Im}[V_{\alpha\beta}^{\text{inel}}(E)] = \int ds \text{Im}[V_{\alpha\beta}^{\text{inel}}(E, s)]. \tag{25}$$

which is Eq. (5) in the main text.